Accepted Manuscript

Structure, surface chemistry and electrochemical de-alloying of bimetallic PtxAg100-x nanoparticles: Quantifying the changes in the surface properties for adsorption and electrocatalytic transformation upon selective Ag removal

Isabella Weber, José Solla-Gullón, Sylvain Brimaud, Juan M. Feliu, R. Jürgen Behm

PII: S1572-6657(16)30689-0
DOI: doi: 10.1016/j.jelechem.2016.11.062
Reference: JEAC 2992

To appear in: *Journal of Electroanalytical Chemistry*

Received date: 30 August 2016
Revised date: 23 November 2016
Accepted date: 25 November 2016

Please cite this article as: Isabella Weber, José Solla-Gullón, Sylvain Brimaud, Juan M. Feliu, R. Jürgen Behm , Structure, surface chemistry and electrochemical de-alloying of bimetallic PtxAg100-x nanoparticles: Quantifying the changes in the surface properties for adsorption and electrocatalytic transformation upon selective Ag removal. The address for the corresponding author was captured as affiliation for all authors. Please check if appropriate. Jeac(2016), doi: 10.1016/j.jelechem.2016.11.062

Structure, surface chemistry and electrochemical de-alloying of bimetallic Pt_xAg_{100-x} nanoparticles: Quantifying the changes in the surface properties for adsorption and electrocatalytic transformation upon selective Ag removal

Isabella Weber[1], José Solla-Gullón[2], Sylvain Brimaud[1,], Juan M. Feliu[2] and R. Jürgen Behm[1]*

[1] Institute of Surface Chemistry and Catalysis, Ulm University,

Albert-Einstein-Allee 47, D-89081 Ulm, Germany

[2] Institute of Electrochemistry, University of Alicante, E-03080 Alicante, Spain

Abstract

We investigated the structure and surface chemistry of bimetallic PtAg nanoparticles, which were prepared by a water-in-oil microemulsion synthesis procedure, as well as the changes therein induced by electrochemical (surface) de-alloying, by a combination of electrochemical and *in situ* FTIR and online differential electrochemical mass spectrometry (DEMS) measurements. Based on transmission electron microscopy the resulting nanoparticles have a narrow size distribution with a mean diameter of around 6 nm, and increasing Ag contents lead to a broadening of the particle size distribution and a loss of the preferential formation of {100} facets observed for Pt nanoparticles. Evaluation of the hydrogen adsorption and CO oxidation characteristics and of the CO adsorption properties (IR) reveals detailed information on the surface composition of the bimetallic nanoparticles before and after electrochemical de-alloying, including also the distribution of Pt and Ag atoms in the surface. Furthermore, relevant information about the modifications in the chemical properties of Pt atoms/sites induced by the presence of Ag is extracted. For the as-prepared nanoparticles we find Ag surface enrichment, while de-alloying results in a core-shell structure with a PtAg core and a Pt shell, whose chemical properties are close to, but not identical, with those of polycrystalline Pt. More general, the study demonstrates that H_{upd} measurements are not suitable to identify the Pt surface content in such kind of bimetallic nanoparticles.

Keywords: Bimetallic nanoparticles, electrochemical de-alloying, segregation, *in situ* spectro-electrochemistry, PtAg, CO electrooxidation

Submitted to: J. Electroanal. Chem. (S.I. A. Aldaz): 30.08.2016

*Author to whom correspondence should be addressed, email: sylvain.brimaud@uni-ulm.de

1. Introduction

Bimetallic, mostly Pt containing nanoparticles have attracted considerable interest in recent years because of their potentially high catalytic activity, which in a number of important electrocatalytic reactions such as the oxygen reduction reaction (ORR) [1,2] or the oxidation of small organic molecules such as CO, methanol or ethanol [3-6] have been shown to exceed that of pure Pt nanoparticles. Studies on structurally well-defined single crystalline planar model electrodes, both experimental and theoretical ones (see, e.g., [7-10]) considerably improved our atomic scale understanding of the physical origin for the high activity. They also revealed the importance of structural modifications, which may be induced by operation under electrochemical reaction conditions, on the resulting catalytic performance [11].

The situation is very different for bimetallic nanoparticles, which are much more relevant for technical applications. For these systems the detailed atomic scale understanding of the ongoing processes is, despite a wealth of kinetic data, including also deactivation / stability measurements, and structural information from electron microscopy, still on a much lower level. This is mainly due to two effects, i) the lack of precise structural information, in particular on the distribution of the components in the particles (3D distribution) and within the surface layer (2D distribution), and ii) the large variety of different local structures present in these samples. The latter results in a large variety of adsorption / reaction sites, which strongly hinders the identification of active structures (‘active site’) and the understanding of restructuring effects on a similar atomic scale. For an improved understanding and to bridge the materials gap it would be highly desirable to map out correlations between structural and electrochemical / electrocatalytic properties for bimetallic Pt containing nanoparticles with a well-defined surface composition, including also the 2D distribution of the components, and to compare these findings with results of studies on related single crystalline planar electrodes. In a similar way, the impact of potential-induced restructuring under

electrochemical conditions on the electrochemical / electrocatalytic properties of the nanoparticle systems should be explored.

This is background of the present work, where we systematically investigated the structure and surface chemistry of bimetallic Pt_xAg_{100-x} nanoparticles with different nominal compositions, which were prepared by a water-in-oil microemulsion method, and changes therein induced by potential cycling (electrochemical de-alloying), employing a combination of electrochemical measurements and *in situ* spectroscopic measurements. This work is part of a comprehensive study on the structure, electrochemical stability and electrochemical/ electrocatalytic properties of bimetallic PtAg electrode materials, following a combined high resolution scanning tunneling microscopy and electrochemistry study on the electrochemical properties and electrochemical restructuring of ultrahigh vacuum (UHV) prepared, structurally well-defined Pt_xAg_{1-x}/Pt(111) monolayer surface alloys [12] and previous experimental and theoretical work on the adsorption characteristics of CO on similar type surfaces [13,14].

In the following, after a brief description of the experimental set-up and procedures (section 2), we will first describe and discuss results on the size / size distribution and on the shape of the resulting nanoparticles obtained from transmission electron microscopy and on the electrochemical properties as derived from voltammetric measurements in supporting electrolyte (section 3.1). Here we also explore the onset of potential induced Ag dissolution and the consequences of potential cycling (electrochemical de-alloying) on the electrochemical characteristics. Next we focus on the CO adsorption behavior on the bimetallic nanoparticles with different compositions, both on the as-prepared samples (before de-alloying) and on the de-alloyed samples, by using *in situ* FTIR spectroscopy (section 3.2). Further information on the CO adsorption characteristic are obtained from potentiodynamic oxidation of pre-adsorbed CO adlayers, where we use online differential electrochemical mass

spectrometry (DEMS) to disentangle Faradaic current contributions from Ag dissolution and from CO_{ad} oxidation (section 3.3). In the discussion, we will make extensive use of our previous findings on related adsorption and electrochemical dissolution processes on structurally well-defined Pt_xAg_{1-x}/Pt(111) monolayer surface alloys [12-14].

2. Experimental

2.1 Preparation of the Pt_xAg_{100-x} nanoparticles

Bimetallic Pt_xAg_{100-x} nanoparticles with different Ag nominal contents ranging between 0-30 at.% were prepared using the water-in-oil (w/o) microemulsion synthesis method described in detail in Ref. [15]. Briefly, the nonpolar phase of the ternary w/o microemulsion, which was prepared first, consisted of 1.571 g (16.5 wt.%) of polyethylene glycol dodecyl ether (Brij® 30, Sigma Aldrich) and 5.471 g (80.5 wt.%) of n-heptane (99 % Scharlau Chemie s.a., extra pure). Aqueous solutions of 0.05 M $H_2PtCl_6 \cdot \times H_2O$ (99.9+ %, Sigma Aldrich) as well as of 0.05 M $AgNO_3$ (99.0-100.5 %, Panreac) were prepared freshly with ultrapure water (MilliQ® water, 18.2 MΩ·cm) containing 25 vol.% of H_2SO_4 (96 %, Merck pro analysi). In total, 0.3 ml (3 wt.%) of a mix of the two metal salt solutions was added to the reaction solution, using the Pt:Ag ratios targeted for. The mixture was stirred continuously until it was macroscopically isotropic and optically transparent. Then, 11.3 mg $NaBH_4$ (10 fold molar excess, 99 %, Sigma Aldrich Reagent Plus) was added quickly. The solution turned black almost instantaneously and was left under stirring for 15 minutes in order to ensure complete reduction. The resulting bimetallic nanoparticles were cleaned by applying a series of successive precipitation and re-dispersion procedures using solvents of increasing polarity [16]. First, the phase separation was induced by the addition of acetone (Panreac, puriss., twofold volume of the synthesis solution). After precipitation of the nanoparticles, the organic supernatant was removed and acetone added once again. After natural sedimentation, this process was repeated again. Five further cleaning and precipitation processes followed (1× acetone, 2× methanol (Merck

Emsure) and 2× ultra-pure water). Finally, the clean particles were stored in ultrapure water. Before the electrochemical experiments, the suspension was ultrasonicated for 10 min.

2.2 Structural characterization

Bright-field transmission electron microscopy (BF-TEM) and energy-dispersive X-ray spectroscopy (EDX) measurements were performed to determine the size, shape and atomic composition of the nanoparticles. A droplet of the dispersed nanoparticle samples was deposited on a Formvar-covered copper grid and evaporated at room temperature in air. The TEM measurements were conducted on a JEOL JEM-2010 microscope (200 kV) coupled with an EDX system (OXFORD INCA Systems).

2.3 Electrochemical characterization

Cyclic voltammograms (CVs) and Ag electrochemical dissolution measurements were performed in a classical three-electrode beaker cell with a platinum wire as counter electrode and a continuously hydrogen-fed reversible hydrogen electrode (RHE) as reference electrode. All potentials in the text refer to the RHE potential scale. For the preparation of the working electrodes, the batches of cleaned nanoparticles which were stored in ultrapure water, were sonicated for 10 min, then a droplet of the dispersed nanoparticle sample (3 µL) was deposited on a polished (Buehler Micropolish II (α-Al_2O_3), 0.3 µm) and electrochemically cleaned glassy carbon disc (ø 3 mm), which was finally dried under a gentle Ar gas flow. No other chemical was added for the preparation of the electrodes since the adhesion of the nanoparticles onto the glassy carbon substrate was sufficient to perform electrochemical measurements. For the experiments we used freshly prepared 0.5 M Ar-saturated (AlphaGaz, 5.0) H_2SO_4 electrolyte solution (96%, Merck Suprapur and ultrapure MilliQ® water (18.2 MΩ·cm)). In order to selectively dissolve Ag from the nanoparticles (electrochemical de-alloying), we applied 10 potential cycles between 0.05 V and 1.45 V at 50 mV s^{-1}. Subsequently, the hydrogen adsorption properties of the (surface) de-alloyed nanoparticles

were probed by cyclic voltammograms between 0.05 V and 0.80 V. An Autolab PGSTAT30 (Metrohm Autolab B. V.) potentiostat interfaced to a computer was employed for potential control and data acquisition. All electrochemical experiments were conducted in Ar-purged, O_2-free electrolyte at room temperature.

2.4 In situ infrared spectroscopy and online mass spectrometric measurements

The CO adsorption and CO electrooxidation properties of the bimetallic particles were studied by *in situ* attenuated total reflection Fourier transform infrared spectroscopy (ATR-FTIRS) combined with simultaneous online differential electrochemical mass spectrometry (DEMS) detection of the CO_2 formed during CO electrooxidation. The experimental setup and procedure for measurements with the nanoparticle samples were described in detail in refs. [17] and [18,19], respectively. This includes also the procedure for the electroless deposition of the Au film serving as electrochemically inert, but electrically conducting support on the internal reflection element (Si prism). *In situ* infrared spectra were recorded using a BioRad FTS 6000 spectrometer equipped with a liquid nitrogen-cooled MCT detector. For online mass spectrometric detection of volatile reaction products we employed a Pfeiffer Vacuum QMS 422 quadrupole mass spectrometer. In these measurements we used an analog Pine Instruments potentiostat (AFRDE-5) interfaced to a computer for potential control and data acquisition.

The vibrational properties of adsorbed CO were probed at a spectral resolution of 4 cm^{-1}. Reference spectra were taken at the same electrode potential prior to adsorption. The acquisition time was set to 120 s per spectrum (400 co-added scans). Spectra are presented in the absorbance mode, *i.e.*, as $A = -\log(R/R_0)$, where R_0 and R are the reflectances at the reference potential in supporting electrolyte and at the sample potential in CO-saturated solution, respectively. Normally, such data processing results in spectra with peaks pointing up for an increased absorption in R with respect to R_0, and peaks pointing down for a loss of

absorption in R compared to R_0, but for nanostructured electrodes an inversion of polarity takes place for IR absorbance spectra (abnormal infrared effect) [20-23]. Saturated CO adlayers were obtained from CO adsorption at constant electrode potential (E = 0.10 V) from CO-saturated electrolyte, subsequently CO was removed from the flow-cell setup by purging it with N_2-saturated electrolyte.

For potentiodynamic oxidative removal of adsorbed CO, the potential was linearly increased (CO_{ad} stripping experiment, 5 mV s^{-1}) and the production of CO_2 was simultaneously tracked by DEMS. The overall procedure was repeated after electrochemical de-alloying carried out with 100 potential cycles between 0.05 V and 1.35 V at 50 mV s^{-1} (the reduced upper potential limit compared to the beaker cell experiments was used to avoid damaging of the Au film). The CO_2 collection efficiencies [24] k* were determined at the end of each new set of DEMS measurements by bulk CO electrooxidation experiments at a constant potential E = 1.35 V.

3 Results and Discussion

3.1 Pt_xAg_{100-x} nanoparticles: structural and electrochemical characterization

Bimetallic Pt_xAg_{100-x} nanoparticles with nominal Ag contents of 0%, 10%, 20% and 30% (atomic composition) were prepared using the water-in-oil microemulsion synthesis method described in section 2.1. In the following, the samples are denominated according to their respective nominal composition, namely Pt_{100}, $Pt_{90}Ag_{10}$, $Pt_{80}Ag_{20}$ and $Pt_{70}Ag_{30}$.

Representative bright-field TEM images of these samples are given in Fig 1. Although the nanoparticles are rather agglomerated, individual nanoparticles are still easily discernible. For the Pt_{100} sample, the nanoparticles are clearly facetted, while with increasing Ag content they become more roundish in shape. Previously, it has been shown that the synthesis procedure employed in the present work favors the formation of {100} facetted Pt nanoparticles, with

the extent of faceting depending on the amount of sulfuric acid in the aqueous phase [15,25]. Thus, for the Pt_{100} sample we expect the current features in the CV in supporting electrolyte to be characteristic for a Pt(100) surface (see below). The presence of the Ag metal salt in the synthesis mixture, which is simultaneously reduced with the Pt salt, apparently reduces the tendency for faceting in the bimetallic Pt_xAg_{100-x} nanoparticles. The histograms in Fig. 1 show that the particle size distributions are rather narrow and monomodal for all nanoparticle samples, independent of the initial Ag content. The presence of more nanoparticles with larger diameter (ca. 8 - 10 nm) in the bimetallic samples results in slightly larger mean particle diameters <d> for the bimetallic Pt_xAg_{100-x} nanoparticle samples (<d> ≈ 6.5 nm) than for the Pt_{100} sample (<d> = 5.9 nm), as derived from a fit of the histograms with a lognormal function (see Fig. 1). Thus, the additional Ag salt in the synthesis mixture also increases the tendency for particle growth, although the effects are not very pronounced.

Further information on the composition of bimetallic nanoparticles is obtained from the EDX analysis (see Table 1). The atomic compositions of the bimetallic samples, as probed by EDX, are very close to the nominal compositions that were targeted. Hence, the water-in-oil microemulsion synthesis method allows for a controlled preparation of bimetallic Pt_xAg_{100-x} nanoparticle samples with desired atomic compositions up to 30% in Ag, while maintaining a narrow particle size distribution. The particles do, however, loose the tendency for (100) faceting with increasing Ag content.

In order to obtain additional information on the surface structure of the nanoparticle samples these were characterized by cyclic voltammetry (CV) in 0.5 M H_2SO_4 supporting electrolyte. To begin with, each sample was subjected to a potential cycling procedure (lower potential limit: 0.05 V, see Fig. S1 in the Supporting Information) with stepwise increased upper potential limit in order to i) determine the potential range where no changes in the current traces occur, indicative of the absence of potential-induced surface restructuring, to ii)

determine the electrode potential at which Ag dissolution is initiated, and to iii) probe the effect of the initial Ag content on the properties of the bimetallic nanoparticles for hydrogen electrosorption. In Fig. 2 we present a set of selected cyclic voltammograms, showing for each sample the two CVs with upper potential limits just below and just above the onset of restructuring and Ag dissolution.

For the Pt_{100} sample (Fig. 2a), where we were mainly interested in the H_{upd} characteristics, the cyclic voltammogram (CV) in 0.5 M H_2SO_4 was recorded between 0.05 V and 0.80 V to avoid any restructuring due to oxide formation / reduction [26]. The CV exhibits the characteristic features of a polycrystalline electrode, with two well-resolved pairs of symmetric peaks centered at 0.12 V and 0.26 V, which have been associated with hydrogen electrosorption on Pt(110) and Pt(100) sites, respectively [16]. Interestingly, the broad contribution between 0.30 V and 0.40 V, characteristic for hydrogen electrosorption on more extended (100) oriented facets [26-28], denote a preferential {100} orientation of the surface structure of these Pt nanoparticle sample (see also [15]).

CVs recorded on the Pt_xAg_{100-x} nanoparticles samples are depicted in Figs. 2b - d. The solid lines represent the CVs with the highest upper potential limit where no change in hydrogen electrosorption has been noticed (see above), the dotted line the subsequent CV, i.e., the CV with the lowest upper limit where changes in the hydrogen region of the CV were observed. The onset potentials for Ag dissolution of each bimetallic nanoparticle samples are indicated by arrows in the corresponding figure. For $Pt_{90}Ag_{10}$ and $Pt_{80}Ag_{20}$, potential-induced Ag dissolution is initiated at ca. 0.86 V and 0.83 V, respectively, while for $Pt_{70}Ag_{30}$ it starts at a significantly lower potential of ca. 0.61 V. Hence, in good agreement with findings from bulk Pt electrodes covered with various amount of surface Ag [29,30] or Pt_xAg_{1-x}/Pt(111) monolayer surface alloys [12], Pt atoms within the bimetallic particles induce a stabilization

of Ag surface atoms against dissolution, and this stabilization decreases with increasing nominal Ag nominal.

It is well known that for bulk Ag electrodes in acid electrolyte, Ag dissolution is initiated at about 0.50 V [29,31]. On the other hand, it has been demonstrated for structurally well-defined Pt_xAg_{1-x}/Pt(111) monolayer surface alloy electrodes that surface Ag atoms are stabilized by adjacent Pt atoms and that for Ag surface contents up to 58 % potential-induced Ag dissolution is inhibited up to 0.95 V [12]. The above results on bimetallic Pt_xAg_{100-x} nanoparticles with different Ag contents, which indicate a higher stability of the bimetallic than observed for bulk Ag electrodes, but a slightly lower stability than observed for the Pt_xAg_{1-x}/Pt(111) monolayer surface alloys, suggest that the surface region of the as-prepared bimetallic samples is more Ag-rich than the $Pt_{42}Ag_{58}$/Pt(111) monolayer surface alloys.

The hydrogen electrosorption features obtained on the bimetallic Pt_xAg_{100-x} nanoparticles (Figs. 2b-d, solid lines), differ significantly from those on the pure Pt_{100} sample. Since the CVs of Ag electrodes are featureless in this potential region [30,32], and considering that hydrogen strongly prefers adsorption on highly coordinated sites, the voltammetric signals in the low potential region are attributed to hydrogen electrosorption on Pt containing surface sites such as Pt_3 sites or Pt_2Ag sites. Furthermore, for hydrogen adsorption on Pt_xAg_{1-x}/Pt(111) monolayer surface alloys we found that under electrochemical conditions only hydrogen adsorption on Pt_3 sites is stable [12]. It is plausible to assume a similar preference also for adsorption on the Pt_xAg_{100-x} alloy nanoparticles. In contrast to hydrogen adsorption on Pt_xAg_{1-x}/Pt(111) monolayer surface alloys, however, the shape of the hydrogen adsorption features changes significantly with Ag content, indicating that the hydrogen adsorption properties of these sites on the bimetallic nanoparticles are somehow affected by the neighborhood of Ag atoms. On $Pt_{90}Ag_{10}$ (Fig. 2b), hydrogen electrosorption takes place between 0.05 V and 0.36 V, with a pair of very broad symmetric peaks centered at ca. 0.22 V.

The Faradaic current for hydrogen electrosorption on the $Pt_{80}Ag_{20}$ nanoparticles (Fig. 2c) is described by an essentially constant current between 0.05 V and 0.20 V, followed by a current decay in the range between 0.2 and 0.33 V. For the $Pt_{70}Ag_{30}$ (Fig. 2d), only a narrow peak with a maximum at 0.07 V remained, which decreases about exponentially and reached the double layer current at 0.29 V. Thus, with increasing Ag content, the coulometric signal associated with hydrogen electrosorption on the highly Pt coordinated sites shifts towards lower electrode potentials, indicative of a lowering of the hydrogen binding energy on these sites (with increasing Ag content).

A similar decrease in hydrogen adsorption energy with increasing Ag (Au) surface content had been observed earlier for hydrogen adsorption on PdAu/Pd(111) [33] and PdAg/Pd(111) [34] surfaces, where it had been assigned to ensemble effects, due to a decreasing hydrogen bond strength on smaller Pt surface ensembles. On the other hand, for structurally well-defined Pt_1Ag_{1-x}/Pt(111) monolayer surface alloys we found that the characteristic feature representing hydrogen adsorption on Pt(111) does not change its potential range, it only decreases with increasing Ag surface content, due to the decreasing abundance of these sites [12]. Hence, in the present case, the decreasing stabilization of hydrogen bound on highly coordinated Pt_n sites must be related to other effects, most likely to a combination of strain effect, due to the increase in the lattice constant with increasing Ag content, and/or to the increasing presence of subsurface Ag atoms, similar to recent findings of a destabilization of CO adsorbed on Pt surface atoms on $Pt_{1-x}Ag_x$/Pt(111) monolayer surface alloys by subsurface Ag atoms [14].

Cyclic voltammograms of the hydrogen region recorded after electrochemical de-alloying, by 100 potential cycles between 0.07 V and 1.35 V at 50 mV s^{-1}, are shown in Fig. 2e. Note that for comparison the Pt_{100} sample was exposed to the same treatment. Regardless of the initial Ag content, the CVs are essentially identical, presenting the same characteristics for hydrogen

electrosorption and exhibiting the same typical current features of a polycrystalline Pt electrode (see above). Apparently, after the de-alloying treatment, the surface / surface near regions of the bimetallic particles are either free of Ag atoms, or these are present at so low concentrations that they cannot be detected by hydrogen electrosorption. This result agrees with previous findings by Strasser and co-workers [35-37], who reported the formation of core-shell particles with a Pt shell on a bimetallic core upon electrochemical de-alloying of Pt-containing bimetallic nanoparticles such as PtNi, PtCo or PtCu, by dissolution of the less noble metal in the surface region. The presence of remaining Ag in the core of the nanoparticles after electrochemical de-alloying of Pt_xAg_{100-x} nanoparticles will be demonstrated in the following sections. Note also that the thickness of the Pt shell resulting in our experiments is not known. It must be thick enough, however, to prevent significant effects of Ag atoms in the core region on the hydrogen electrosorption properties of surface Pt sites.

The coulometric charges determined from hydrogen desorption before and after electrochemical de-alloying of the Pt_xAg_{100-x} nanoparticle samples are summarized in Table 1. Considering that the absolute amount of deposited nanoparticles was hard to control precisely, we will focus on the ratio of the hydrogen desorption charges before and after de-alloying, which is listed in the last column of table 1. Since these values were obtained on the same electrodes for each nanoparticle sample, the metal loading is identical before and after de-alloying. The absolute values obtained for the different samples and changes therein with increasing Ag content will be discussed in more detail in section 3.3, together with the results of the CO_{ad} stripping measurements.

For Pt_{100}, the hydrogen desorption charge remains essentially unchanged upon the de-alloying procedure, indicating the absence of any substantial roughening or loss of material during this treatment. With increasing Ag, content, this ratio decreases, i.e., the hydrogen desorption charge and therefore the total amount of hydrogen adsorbed on the as prepared samples,

relative to that on the de-alloyed samples, down to 14% of the value for the de-alloyed nanoparticles for the $Pt_{70}Ag_{30}$ sample (Table 1).

These changes point to a rapidly decreasing Pt content in the surface layer with increasing nominal Ag content in the bimetallic nanoparticles. For evaluating the surface composition of the bimetallic nanoparticles, we will, in a first order approximation, assume that the Pt surface content scales approximately linearly with the amount of hydrogen adsorption, i.e., with the hydrogen adsorption charge. Considering that under present conditions H adsorption is likely to be stable only on highly Pt coordinated sites (see above), one would expect a distinctly non-linear relation between surface Pt content and H adsorption. A recent combined UHV-STM electrochemical study on structurally well-characterized Pt_xAg_{1-x}/Pt(111) monolayer surface alloys revealed, however, that these two properties are almost linearly correlated, which is largely due to the pronounced tendency for phase segregation on these surface alloys [12]. In the absence of similar structural data on the present bimetallic Pt_xAg_{100-x} nanoparticles we will assume a similar tendency also for these nanoparticles. This is a rough approximation which will become evident when discussing the CO_{ad} stripping data in section 3.3. Furthermore, we will assume for the moment that after de-alloying all samples exhibit a surface comparable to polycrystalline Pt surface, which is justified by the similar appearance of the H_{upd} current traces after de-alloying (see Fig. 2e). We will return to this point, however, in section 3.3.

For determining the content of Ag atoms in the surface layer we furthermore have to consider the slight increase in mean particle size, from 5.9 nm (Pt_{100}) to about 6.5 nm for the bimetallic Pt_xAg_{100-x} nanoparticles. Using the (simplified) assumption of a linear correlation between hydrogen adsorption charge and Pt surface content and considering that i) the total number of atoms in a 6.5 nm noble metal nanoparticle is roughly 12000 and ii) the fraction of surface atoms, relative to the total number of atoms in a (spherical) nanoparticle, the dispersion D, is

approximately equal to the inverse of the particle diameter in nm [38,39], we can estimate that the Ag surface content in the as prepared bimetallic nanoparticles is around 45%, 79% and 86% for the $Pt_{90}Ag_{10}$, $Pt_{80}Ag_{20}$ and $Pt_{70}Ag_{30}$ nanoparticle samples, respectively. These values represent the maximum Ag surface contents, assuming a linear relation between hydrogen desorption charge density and Pt surface content; any deviation to a non-linear relation with an initially faster decay of the H_{upd} charge with Pt surface concentration would result in lower values. We will demonstrate later (section 3.3) that this assumption is not fully correct for PtAg nanoparticles and leads to an overestimation of the surface Ag surface content. Nevertheless, it is useful for a rough qualitative estimation of the Ag surface segregation after electrochemical measurements in beaker cell. The above values mean that 70%, 61% and 44% of the initial Ag content of the respective samples are located at the surface of the as-prepared nanoparticle samples, as a result of the synthesis process/method employed. This amount of Ag surface atoms should reflect also the minimum Ag content that we can expect to be removed from the bimetallic nanoparticles during the electrochemical de-alloying process.

The above results indicate a strong tendency for surface segregation of Ag atoms in the bimetallic Pt_xAg_{100-x} nanoparticles during the synthesis procedure. A similar tendency was observed also for PtAg nanoparticles prepared by other colloidal method [40], and is in good agreement also with a detailed structural analysis of bimetallic PtAg nanoparticles prepared by the polyol method [41]. Although a quantitative comparison between the two phenomena is hardly possible, it should be noted that a tendency for two-dimensional phase separation was observed also in an STM study of Pt_xAg_{1-x}/Pt(111) monolayer surface alloys prepared under UHV conditions [12,42].

Table 1: Nominal sample compositions, Pt and Ag atomic percentages obtained from EDX analyses (before electrochemical de-alloying), coulometric charges for hydrogen

desorption before and after the electrochemical de-alloying process, respectively, and ratio between these values.

Nominal sample composition	EDX analysis		Coulometric charge for hydrogen desorption / µC		Ratio of hydrogen desorption charges before and after de-alloying
	at.% Pt	at.% Ag	before de-alloying	after de-alloying	
Pt_{100}	100	-	107	108	0.99
$Pt_{90}Ag_{10}$	90	10	49	89	0.55
$Pt_{80}Ag_{20}$	82	18	15	72	0.21
$Pt_{70}Ag_{30}$	73	27	9	62	0.14

3.2. IR vibrational properties for adsorbed CO

The vibrational properties of a saturated CO adlayer, which was adsorbed at E = 0.10 V on the surface of the Pt_xAg_{100-x} nanoparticles, were characterized by *in situ* IR spectroscopy before and after electrochemical de-alloying. Note that the same treatment was applied also to the Pt_{100} electrode for comparison. The resulting IR spectra (CO_{ad} vibrational region only), recorded at E = 0.10 V in CO-free electrolyte, are depicted in Fig. 3. In all cases the IR bands characteristic for adsorbed CO are more intense after the de-alloying process than before. Furthermore, even when considering variations in the metal loading of the electrodes, they seem to decrease with increasing initial Ag content, both for IR probing before and after the de-alloying process. It should be noted already at this point that in particular for the de-alloyed samples the loss in intensity is much more pronounced than expected from the decreasing amount of CO_{ad}, which was determined by CO_{ad} oxidation (see section 3.3). This is attributed to pronounced sensitivity effects in the IR measurements.

For the initial Pt_{100} sample (Fig. 3a), before the electrochemical de-alloying treatment, the IR vibrational properties for CO_{ad} are very similar to those reported for shape-selected Pt nanoparticles with preferential {100} surface structure, with two clearly resolved IR bands at 2067 cm^{-1} and 1878 cm^{-1}, which were attributed to linearly (CO_l) and bridge-bonded (CO_b) adsorbed CO, respectively [43]. After the electrochemical de-alloying treatment, the IR spectrum for CO_{ad} is very similar to that obtained for CO adsorbed on polycrystalline electrodes [18], with CO_l and CO_b bands at 2069 cm^{-1} and 1869 cm^{-1}, respectively, and a significantly lower (relative) intensity of the CO_b band than before. These results agree well with the close similarity of the hydrogen electrosorption properties of the de-alloyed nanoparticles and of polycrystalline Pt (see CVs in Fig. 2e).

Going to the bimetallic electrodes, we first want to note that in previous *in situ* IR studies on bulk Ag electrodes, CO_{ad} related IR bands were observed only in CO-saturated electrolyte

[44], suggesting that CO_{ad} is only weakly adsorbed on pure Ag surfaces and in dynamic equilibrium with CO in solution. Since the IR spectra are recorded in CO-free solution, we attribute the IR bands for CO_{ad} on the Pt_xAg_{100-x} nanoparticle samples to CO adsorbed on surface Pt atoms and sites. Considering the weak bonding to mixed PtAg sites obtained in recent DFT based calculations [14], CO_l and CO_b must be bound to 1 Pt surface atom and to pairs of 2 adjacent Pt surface atoms, respectively.

For the as prepared $Pt_{90}Ag_{10}$ and $Pt_{80}Ag_{20}$ samples, before electrochemical de-alloying, only a single IR band attributed to CO_l is observed, which is located at 2055 cm^{-1} and 2040 cm^{-1}, respectively. For $Pt_{70}Ag_{30}$ the CO_l related IR band hardly emerges from the background noise. The rapid decrease in the IR band intensity with increasing initial Ag content agrees at least qualitatively with the increasing fraction of Ag surface atoms in the bimetallic nanoparticle surfaces (see section 3.1). On a quantitative scale, however, the decay of the IR band intensities is much more pronounced than expected, considering that significant amounts of CO are adsorbed on the PtAg nanoparticles even for high Ag nominal contents (see section 3.3). This also points to the presence of distinct sensitivity effects, as suggested above for the de-alloyed samples. A more detailed discussion of these effects is, however, beyond the scope of the present communication. The band shift towards lower wavenumbers indicates that compared to pure Pt nanoparticle sample, the adsorbed CO is more strongly bound at the bimetallic nanoparticles, and that the CO bond strength increases with the initial Ag content. This result is in good agreement with recent findings from combined temperature programmed desorption / infrared spectroscopy studies on CO adsorption on well-defined Pt_xAg_{1-x}/Pt(111) surface alloys, which showed that for Ag surface contents higher than 50% a stabilized state CO_{ad} state was formed. This was attributed to CO adsorbed on individual Pt surface atoms surrounded by Ag atoms, where the bond between Pt and CO_{ad} is stabilized by lateral ligand effects [14]. Hence, the observation of stabilized CO_{ad} is in good agreement with the conclusion of high Ag surface concentrations on the as prepared bimetallic samples.

A further stabilization would result from strain effects, due to increasing lattice size of the bimetallic core with increasing Ag content. On the other hand, previous experiments and calculations showed a weakening of the Pt-CO bond in the presence of subsurface Ag atoms [14], which may contribute as well for higher Ag concentrations (30%).

IR spectra of CO_{ad} on the bimetallic Pt_xAg_{100-x} nanoparticle samples recorded after electrochemical de-alloying are more complex than those obtained on the as-prepared samples, as they show several IR bands related to CO_l species. This points to a larger variety of surface sites with different CO adsorption properties. In that respect, they differ also from those obtained for CO adsorbed on Pt_{100} nanoparticle samples, where only a single band was observed for CO_l. For the de-alloyed bimetallic Pt_xAg_{100-x} nanoparticle samples, the characteristic IR band for CO_b is shifted by ca. 15 cm^{-1} to lower wavenumbers with respect to Pt_{100}, independent of the initial Ag content of the bimetallic nanoparticles. Furthermore, the relative intensity of the CO_b band, relative to that of the CO_l bands, increased with growing initial Ag content in the bimetallic nanoparticles. Finally, for all three bimetallic samples we find three IR bands, one at 2069 cm^{-1}, at a similar position as in the Pt_{100} sample, and two at lower wavenumbers, e.g., at 2015 cm^{-1} and 2032 cm^{-1} for the $Pt_{90}Ag_{10}$ sample. Obviously, only part of the Pt surface exhibit the same CO adsorption properties as the Pt_{100} sample, which gives rise for an IR band at 2069 cm^{-1}. The relative intensity of the IR band at 2069 cm^{-1} compared to those of the other two bands decreases significantly with increasing Ag content, and for the de-alloyed $Pt_{70}Ag_{30}$ sample, it has disappeared in the foot of the band lower frequency band. Hence, the fraction of Pt surface sites with polycrystalline Pt like CO adsorption properties decreases with increasing Ag content. At the same time, the lower frequency bands shift slightly to lower wavenumbers, from 2015 cm^{-1} and 2032 cm^{-1} for the $Pt_{90}Ag_{10}$ sample to at 2012 cm^{-1} and 2027 cm^{-1} for the $Pt_{70}Ag_{30}$ sample. Overall, these trends are a clear indication that the remaining Ag content after electrochemical de-alloying, either in the core or in the shell of the nanoparticles, has a distinct effect on the CO adsorption

properties on the Pt_xAg_{100-x} nanoparticle samples, although they all exhibit voltammetric features for hydrogen electrosorption similar to those of the Pt_{100} nanoparticle sample (see previous section). This particular point will be discussed in more detail below (section 3.3).

These differences may at least partly be due to strain effects. Previous X-ray diffraction measurements had shown that bimetallic PtAg nanoparticles have a larger lattice constant than Pt, in good agreement with what would be expected according to Vegard's law [41], and therefore the Pt shell formed after electrochemical de-alloying [36,37] should experience tensile strain, assuming pseudomorphic structure of the Pt shell on the lattice of the bimetallic core. According to the d-band model a larger Pt-Pt distance goes along with a stronger bond of adsorbed species [45], and in the case of adsorbed CO, with a red-shift in the IR bands for CO_{ad}. This seems to agree with the experimental observations, specifically with the formation of two bands at lower wavenumbers on the de-alloyed bimetallic samples. On the other hand, however, the band typical for CO_l on Pt_{100}, at 2069 cm^{-1}, is present also on the de-alloyed bimetallic samples, though with rapidly decreasing intensity, both on an absolute and on a relative scale, relative to other bands. Since it is well know that IR band intensities of adsorbed species, in particular of CO_{ad}, are far from giving a quantitative account of the respective adsorbate coverages, it is not possible to quantify the fraction of sites identical with the Pt_{100} sample and of lower frequency Pt adsorption sites on the de-alloyed bimetallic samples, and the same is true also for the exact nature of the lower frequency sites. These questions will be discussed more in the next section, after presenting the CO_{ad} stripping data.

3.3. CO adlayer stripping

Finally we investigated the influence of the Ag content in the Pt_xAg_{100-x} nanoparticles on the potentiodynamic oxidation of a saturated CO adlayer (CO_{ad} stripping), which had been adsorbed at 0.10 V. These measurements were performed both before and after electrochemical de-alloying, using the same electrode for each sample. The resulting current

traces for CO oxidation (Faradaic current) and CO_2 formation (partial current for CO_2 formation, j_{CO2}) are presented in Fig. 4. The latter was obtained by normalization of the mass spectrometric ion current (m/z = 44), which was recorded simultaneously to the Faradaic current, by the CO_2 collection efficiency (see section 2.4 and Ref. [19]). The conversion of currents into Pt surface area normalized current densities will be discussed below.

For Pt_{100}, the CO oxidation starts at ca. 0.32 V with a pre-peak, followed by the main oxidation peak centered at 0.67 V and a second oxidation peak at 0.72 V (Fig. 4a). This result is in very good agreement with CO_{ad} stripping current traces on nanoparticles with preferential (100) orientation [19,26,27,46]. The oxidation peak at high potentials is characteristic for ordered (100) domains on the surface of the Pt nanoparticles [46]. Moving to $Pt_{90}Ag_{10}$ (Fig. 4b), the current trace for CO_{ad} stripping exhibits two peaks centered at 0.80 V and 1.12 V, while the partial current for CO_2 detection shows only a single peak at 0.80 V. Accordingly, we attribute the peak at 1.12 V to potential-induced Ag dissolution. A similar result is found for CO_{ad} stripping on $Pt_{80}Ag_{20}$ (Fig. 4c), but the CO_{ad} oxidation peak is shifted by 0.11 V to higher potentials, to 0.91 V, with a shoulder at lower potential (0.81 V), and the current associated with Ag dissolution is significantly larger. This latter behavior agrees well with the larger Ag content and in particular the higher content of surface Ag atom of this sample compared to $Pt_{90}Ag_{10}$ (see section 3.1).The much higher potential for Ag dissolution obtained for these samples compared to Ag bulk dissolution in acidic electrolyte also points to a Pt-induced stabilization of Ag atoms in the bimetallic Pt_xAg_{100-x} nanoparticles samples in acidic electrolyte discussed before (section 3.1). Interestingly, however, this peak does not shift to higher potentials with increasing Ag content. For the $Pt_{70}Ag_{30}$ nanoparticles (Fig. 4d), three current peaks are resolved in the CO_{ad} stripping current trace, at 0.72, 0.93 and 1.12 V, respectively, while the CO_2 formation current exhibits only a single peak at 0.93 V, with a small shoulder at lower potentials. Hence, for $Pt_{70}Ag_{30}$ the current peaks at 0.72 and 1.12 V

must be due to Ag dissolution. The peak at 0.72 V is assigned to dissolution of Ag which was less stabilized by neighboring Pt atoms than that dissolving in the peak centered at 1.12 V.

The continuous shift of the main CO_{ad} oxidation peak to higher potentials with increasing initial Ag content in the nanoparticles agrees well findings from IR spectroscopy (see Fig. 3), which indicated a stronger binding of the adsorbed CO as the fraction of Ag in the bimetallic $Pt_{100-x}Ag_x$ nanoparticle samples increased.

The second positive-going potential scans (grey lines in the top panels in Figs. 4b - d), recorded after complete removal of the CO adlayer, show the recovery of the hydrogen region. For the bimetallic Pt_xAg_{100-x} nanoparticle samples, the current signals in the hydrogen region differ significantly from those obtained in initial CVs with the upper potential limit kept below the onset of Ag dissolution (compare with Figs. 2b-d), which demonstrates that CO_{ad} stripping in the first positive-going potential scan is accompanied by partial dissolution of surface Ag. For more information on this process we calculated the partial current for Ag dissolution in the first positive-going current scan, during COad oxidation, by subtracting the partial current for CO_2 formation from the total Faradaic current (note that the CO_2 formation current was multiplied by a factor of ~1.2 to account for re-adsorption of sulphate [19]). The resulting Ag dissolution currents are illustrated as full lines in Fig. 5.

Similar experiments were performed on the different Pt_xAg_{100-x} nanoparticle samples after electrochemical de-alloying. The resulting Faradaic current and CO_2 formation current densities (see Fig. S2 in the Supporting Information) closely resemble each other in the H_{upd} region (2^{nd} positive going scan) and in the Pt oxidation region, as expected samples with largely identical, Pt like surfaces. They do reveal, however, slight systematic differences in the CO_{ad} oxidation signals. This is illustrated more clearly in Fig. 6, where we collected the mass spectrometric current traces for CO_2 formation of the different Pt_xAg_{100-x} samples. In all cases, CO_{ad} oxidation starts with an oxidation pre-peak, whose onset shifts from ca. 0.32 to

0.38 V with increasing initial amount of Ag (0 - 30 at.%) in the nanoparticles. A similar shift occurs also for the peak center, which shifts from 0.66 V to 0.67 V, 0.69 V and 0.71 V for Pt_{100}, $Pt_{90}Ag_{10}$, $Pt_{80}Ag_{20}$ and $Pt_{70}Ag_{30}$, respectively. Finally, there is a small second oxidation peak at 0.80 V in the current trace of the $Pt_{70}Ag_{30}$ sample. Obviously, the influence of the remaining (surface) Ag on the CO electrooxidation behavior of the de-alloyed nanoparticles is much less pronounced than before electrochemical de-alloying, but still present. This agrees well with our findings for the vibrational properties of CO_{ad}, which also indicated Ag induced modifications of the CO adsorption properties of the de-alloyed bimetallic samples compared to the de-alloyed Pt_{100} sample (see section 3.2).

Finally we will discuss trends in the coulometric charge densities for CO_{ad} oxidation (Q_{CO}) and, for comparison, for hydrogen desorption (Q_H) derived from these measurements, both for the as-prepared (Q_{ap}) and for the de-alloyed (Q_{da}) samples. From similar reasons as discussed before we will focus on values which are independent of the absolute metal loading such as the charge ratios Q_H/Q_{CO} and Q_{da}/Q_{ap}, and finally derive charge densities normalized to the overall metal surface area. These values are collected in Table 2.

The coulometric charge q_{CO} for oxidative removal of a CO adlayer on Pt_{100} is unaffected by the electrochemical de-alloying procedure ($q_{CO,da}/q_{CO,ap}$ = 1.01). (Note that the currents for CO oxidation (CO_2 formation) were calculated from the mass spectrometric CO_2 ion currents using the respective k* factors (see experimental section 2.4)). Furthermore, both for the as-prepared and for the de-alloyed sample we obtained values of 1.42 for the ratio of CO oxidation vs. hydrogen desorption charge (Q_{CO}/Q_H), which corresponds exactly to what would be expected considering that the experimentally derived hydrogen desorption charge (210 µC cm^{-2} for saturation coverage (0.7 monolayers (ML)) contains contributions from sulphate re-adsorption (60 µC cm^{-2}) [47] and that CO_{ad} oxidation (saturation coverage 0.7 ML [19]) contributes 2 electrons per molecule CO_{ad}. Focusing now on the de-alloyed samples, the ratio

$q_{CO,da}/q_{H,da}$ increases slightly with increasing Ag content, from 1.42 to 1.55. Since these charges refer to the same electrode, this means that either the CO adsorption charge density increases with increasing Ag content, or that the hydrogen desorption charge decreases slightly with increasing Ag content. Considering that these surfaces still somehow feel the presence of Ag, as evidenced by the *in situ* IR measurements, we find the latter possibility more plausible, since the presence of surface or subsurface Ag may result in weakly hydrogen bonding adsorption sites, which will not be populated at room temperature, while CO adsorption with its much stronger bond will be little affected [14]. In addition, CO adsorption is also possible on Pt monomers and Pt_2 dimers surrounded by Ag surface atoms [14], while this is not possible for hydrogen [12]. Considering also that all de-alloyed surfaces exhibit the electrochemical characteristics of polycrystalline Pt we decided to use the CO_{ad} oxidation charge for determining the Pt surface area of the de-alloyed samples, which should be identical to the overall metal surface area. Using a value of 300 µC cm^{-2}_{Pt}, this results in charge densities for hydrogen desorption of between 211 µC cm^{-2}_{Pt} (Pt_{100}) and 194 µC cm^{-2}_{Pt} ($Pt_{70}Ag_{30}$).

For calibration of the current densities obtained on the as-prepared nanoparticles we assume that the metal loading and hence the surface area does not change significantly upon electrochemical de-alloying, i.e., we neglect changes therein due to material losses during de-alloying surfaces, which is supported by the results obtained on Pt_{100} sample. With this assumption, we obtain the metal surface area normalized current densities for CO_{ad} oxidation (Q_{CO}) and for hydrogen desorption (Q_H) listed in Table 2.

Table 2: Ratio of the coulometric charges for oxidation of a saturated CO adlayer (q_{CO}) and for hydrogen desorption (q_H), where the former is calculated from the mass spectrometric DEMS signal and the latter is derived from the total Faradaic current in the H_{upd} region, and the charge densities derived for saturated CO adlayer

oxidation (Q_{CO}) and hydrogen desorption (Q_H) assuming a charge density of 300 μC cm^{-2} for the de-alloyed samples with their polycrystalline like structure. The charge densities are calculated using the data in Table S1 in the Supporting Information.

Nanoparticle sample	Before de-alloying			After de-alloying		
	q_{CO}/q_H	Q_H μC cm^{-2}	Q_{CO} μC cm^{-2}	q_{CO}/q_H	Q_H μC cm^{-2}	Q_{CO} μC cm^{-2}
Pt_{100}	1.42	209	298	1.42	211	300
$Pt_{90}Ag_{10}$	1.57	165	258	1.48	203	300
$Pt_{80}Ag_{20}$	2.69	82	221	1.50	200	300
$Pt_{70}Ag_{30}$	4.40	54	237	1.55	194	300

These data can be used also to estimate more precisely the Ag contents in the surface of the as prepared samples. For this we assume that at saturation the CO_{ad} coverage per Pt surface atom is constant, i.e., independent of the Ag surface concentration. This is not fully correct, since a Pt monomer or a Pt_2 dimer surrounded by Ag surface atoms will adsorb 1 or 2 CO molecules, corresponding to a local coverage of 1, while for polycrystalline Pt samples, e.g. Pt_{100} samples after potential cycling, saturation coverages of 0.7 have been measured, see the coulometric analysis Table 2. This means that for highly dispersed distributions of Pt surface atoms the actual concentration of Pt surface atoms is lower than what is obtained when using the above assumption, while for 2D phase segregated surfaces with large domains of Pt and Ag atoms deviations should be little. With this approximation we obtain Pt (Ag) surface concentrations of 0.86 (0.14), 0.74 (0.26) and 0.79 (0.21) for the as-prepared $Pt_{90}Ag_{10}$, $Pt_{80}Ag_{20}$ and $Pt_{70}Ag_{30}$ samples, which can be considered as upper (lower) limit for the concentration of Pt (Ag) surface atoms. Even when considering that because of our above simplifications the Pt concentration would be 10%, the resulting values for the Pt (Ag) surface concentration are far

above (below) those obtained from a linear correlation between H desorption charge and Pt surface concentration as done in our first approach in section 3.1).

These results, in particular the non-linear correlation between hydrogen desorption charge q_H and CO oxidation charge q_{CO}, clearly demonstrate that the hydrogen desorption charge is little suited for determining the Pt surface concentration in such kind of bimetallic Pt alloy systems, with a mixed surface composition. This is due to the fact that at room temperature H_{ad} adsorption is only stable on Pt_3 trimer sites, while on Pt_2Ag and Pt_1Ag_2 sites it desorbs. Therefore, dispersed Pt atoms and dimers will not contribute to the hydrogen desorption charge. CO adsorption, in contrast, is stable also on the latter species, hence, they will contribute to the CO_{ad} oxidation charge. The data also demonstrate that in the present case the Pt (Ag) atoms are rather dispersed in the surface layer of the Pt_xAg_{100-x} nanoparticles, since for large domains effects as described above should play a much smaller role than observed here. The results also demonstrate the ambiguity of the term 'electroactive surface area' and the values determined for this for bimetallic surfaces, since they may sensitively depend on the electrochemical / electrocatalytic process considered. These results also illustrate the importance of detailed information on the 2D distribution of surface atoms, since this may significantly affect the (electro-)chemical / (electro-)catalytic properties via ensemble effects.

The above data leave us with the question for the physical origin of the slight, but clearly measurable decay in the hydrogen adsorption charge density (Q_H) with increasing initial Ag content on the de-alloyed bimetallic samples. Looking at the shape of the H_{upd} current traces (see Fig. 2) there is no significant difference between these surfaces. On the other hand, both the CO_{ad} stripping traces (see Fig. 6) as well as the IR spectra of adsorbed CO (Fig. 4) indicate subtle, but clearly resolved differences, as evidenced by the appearance and increasing relative intensity of new CO_l related bands at lower wavenumbers and by a change in CO_l to CO_b intensity. Possible reasons for such modifications may be strain effects, caused

by the larger lattice of the bimetallic PtAg core with increasing Ag content [41], provided the Pt shell is pseudomorphic on the PtAg core, as it is generally assumed for sufficiently thin shell layers in such systems. Similar conclusion were derived from electrochemical investigations on bimetallic $Pt_3M(111)$ bulk electrodes covered by a Pt skin (Pt skin electrodes) [48]. Another possibility would be the presence of remaining surface Ag species, which affect the hydrogen adsorption. At present, we cannot distinguish between these possibilities, and possibly also other ones.

4. Conclusion

We have investigated the structure and surface chemistry as well as the changes therein induced by electrochemical (surface) de-alloying of bimetallic PtAg nanoparticles, which were prepared by a water-in-oil microemulsion synthesis procedure, by spectro-electrochemical measurements. Combining results of electrochemical measurements with *in situ* FTIR and online DEMS measurements performed under continuous electrolyte flow, we arrive at the following conclusions:

1. The water-in-oil microemulsion synthesis method allows for the controlled preparation of bimetallic Pt_xAg_{100-x} nanoparticles with narrow size distribution (here around 6 nm) and nominal Ag contents at least up to 30 at.%. Under conditions used in this work, the synthesis procedure results in a significant surface segregation of Ag atoms, at least for the $Pt_{90}Ag_{10}$ and $Pt_{80}Ag_{20}$ samples.
2. The preference for {100} facets seen for pure Pt nanoparticles is increasingly lost for bimetallic nanoparticles.
3. Electrochemical de-alloying, by cycling to 1.35 V or 1.45 V, results in more or less pure Pt surfaces with hydrogen adsorption properties identical to those of polycrystalline Pt, while CO adsorption and CO oxidation indicate small but clearly significant differences.

This points to the formation of a Pt shell / PtAg core structure of the de-alloyed bimetallic Pt_xAg_{100-x} nanoparticles, where the Pt shell is suggested to experience tensile strain.

4. Ag surface / surface near atoms are stabilized by Pt against dissolution in acid electrolyte, as evidenced by the higher potential required for Ag dissolution from the bimetallic Pt_xAg_{100-x} nanoparticles compared to Ag dissolution from Ag bulk electrodes, in good agreement with previous findings for Pt_xAg_{1-x}/Pt(111) monolayer surface alloys.
5. On the bimetallic Pt_xAg_{100-x} nanoparticles, CO_{ad} oxidation and Ag dissolution occur simultaneously during potentiodynamic CO_{ad} stripping, contributing both to the measured Faradaic current, but can be separated quantitatively by online mass spectrometric (DEMS) detection of CO_2.
6. From the increasing difference between CO_{ad} oxidation charge and hydrogen desorption charge on the as-prepared bimetallic Pt_xAg_{100-x} nanoparticles with increasing Ag content we conclude that Pt and Ag surface atoms must be present in a rather dispersed distribution. This is based on previous findings that CO can adsorb also on Pt_1 and Pt_2 monomers and dimers, while adsorbed hydrogen (H_{ad}), which adsorbs on highly coordinated sites, is not stable on Pt_2Ag, $PtAg_2$ sites ('ensemble effects'). Therefore hydrogen adsorption does not sense Pt surface atoms not included in Pt_3 sites. Differences between the amounts of H adsorption and CO adsorption grow with increasingly dispersed distributions of surface atoms.
7. The presence of adjacent Ag surface atoms ('lateral ligand effects') as well as strain effects result in stronger bonding of CO on Pt surface atoms, while a weakening of the hydrogen binding on the as prepared Pt_xAg_{100-x} nanoparticles is attributed to a more dominant contribution from subsurface Ag atoms ('vertical ligand effects'), in agreement with previous findings in model studies on well-defined Pt_xAg_{1-x}/Pt(111) monolayer surface alloys.

Overall, this study clearly demonstrates the potential of combined electrochemical and *in situ* spectroscopic detection for the atomic scale characterization of bimetallic nanoparticles in general, giving detailed insight into structural and electronic/chemical properties of the nanoparticle surfaces, and specifically that adsorption of hydrogen (H_{upd}) is not a suitable method for determining the Pt surface content in such kind of bimetallic nanoparticles.

Acknowledgements

This work was supported by the Deutsche Forschungsgemeinschaft via the project BE 1201 / 17-1 and by the Ministerio de Economía y Competitividad (project CTQ2013-44083-P) and Generalitat Valenciana (project PROMETEOII/2014/013).

References

1. U.A. Paulus, A. Wokaun, G.G. Scherer, T.J. Schmidt, V. Stamenkovic, V. Radmilovic, N.M. Markovic, and P.N. Ross Jr., *Oxygen reduction on carbon-supported Pt-Ni and Pt-Co alloy catalysts* J. Phys. Chem. B 106 (2002) 4181-4191

2. V. Stamenkovic, T.J. Schmidt, P.N. Ross, and N.M. Markovic, *Surface composition effects in electrocatalysis: Kinetics of oxygen reduction on well-defined Pt_3Ni and Pt_3Co alloy surfaces* J. Phys. Chem. B 106 (2002) 11970-11979

3. O.A. Petrii, *Pt–Ru electrocatalysts for fuel cells: a representative review* J. Solid State Electrochem. 12 (2008) 609-642

4. C. Lamy, J.-M. Léger, and S. Srinivasan, in *Modern Aspects of Electrochemistry*, J. O. Bockris, B. Conway, and R. E. White, Eds. (Kluwer Academic/Plenum Publishers, New York, 2001), Vol. 34.

5. C. Lamy, E.M. Belgsir, and J.-M. Léger, *Electrocatalytic oxidation of aliphatic alcohols: Application to the direct alcohol fuel cell (DAFC)* J. Appl. Electrochem. 31 (2001) 799-809

6. C. Lamy, S. Rousseau, E.M. Belgsir, C. Coutanceau, and J.-M. Léger, *Recent progress in the direct ethanol fuel cell: development of new platinum-tin electrocatalysis* Electrochim. Acta 49 (2004) 3901-3908

7. V.R. Stamenkovic, B.S. Mun, M. Arenz, K.J.J. Mayrhofer, C.A. Lucas, G. Wang, P.N. Ross, and N.M. Markovic, *Trends in electrocatalysis on extended and nanoscale Pt-bimetallic alloy surfaces* Nature Mater. 6 (2007) 241-247

8. A.S. Bandarenka, A.S. Varela, M. Karamad, F. Calle-Vallejo, L. Bech, F.J. Perez-Alonso, J. Rossmeisl, I.E.L. Stephens, and I. Chorkendorff, *Design of an active site towards optimal electrocatalysis: Overlayers, surface alloys and near-surface alloys of Cu/Pt(111)* Angew. Chem. Int. Ed. 51 (2012) 11845-11848

9. T.P. Johansson, E.T. Ulrikkeholm, P. Hernandez-Fernandez, P. Malacrida, H.A. Hansen, A.S. Bandarenka, J.K. Nørskov, J. Rossmeisl, I.E.L. Stephens, and I. Chorkendorff, *Pt skin versus Pt skeleton structures of Pt_3Sc as electrocatalysts for oxygen reduction* Top. Catal. 57 (2014) 245-254

10. S. Brimaud, A.K. Engstfeld, O.B. Alves, and R.J. Behm, *Structure-reactivity correlation in the oxygen reduction reaction: Activity of structurally well defined $Au_xPt1\text{-}x/Pt(111)$ monolayer surface alloys* J. Electroanal. Chem. 716 (2014) 71-79

11. A.K. Engstfeld, S. Brimaud, and R.J. Behm, *Structural characterization of model electrodes: A must in electrocatalysis research* Angew. Chem. Int. Ed. 53 (2014) 12936-12940

12. S. Beckord, A.K. Engstfeld, S. Brimaud, and R.J. Behm, *Electrochemical characterization and stability of $Ag_xPt_{1-x}/Pt(111)$ surface alloys* J. Phys. Chem. C 120 (2016) 16179-16190

13. T. Diemant, K.M. Schüttler, and R.J. Behm, *Ag on Pt(111): Changes in electronic and CO adsorption properties upon PtAg/Pt(111) monolayer surface alloy formation* Chem. Phys. Chem. 16 (2015) 2943-2952

14. K.M. Schüttler, L.A. Mancera, T. Diemant, A. Gross, and R.J. Behm, *Interaction of CO with $Pt_xAg_{1-x}/Pt(111)$ surface alloys: More than dilution by Ag atoms* Surf. Sci. 650 (2016) 237-254

15. R.A. Martinez-Rodriguez, F.J. Vidal-Iglesias, J. Solla-Gullón, C.R. Cabrera, and J.M. Feliu, *Synthesis and electrocatalytic properties of H_2SO_4-induced (100) Pt nanoparticles prepared in water-in-oil microemulsion* ChemPhysChem 15 (2014) 1997-2001

16. J. Solla-Gullón, V. Montiel, A. Aldaz, and J. Clavilier, *Electrochemical characterisation of platinum nanoparticles prepared by microemulsion: how to clean them without loss of crystalline surface structure* J. Electroanal. Chem. 491 (2000) 69-77

17. M. Heinen, Y.X. Chen, Z. Jusys, and R.J. Behm, *In situ ATR-FTIRS coupled with on-line DEMS under controlled mass transport conditions - A novel tool for electrocatalytic reaction studies* Electrochim. Acta 52 (2007) 5634-5643

18. S. Brimaud, Z. Jusys, and R.J. Behm, *Controlled surface structure for in-situ ATR-FTIRS studies using preferentially shaped Pt nanocrystals* Electrocatal. 2 (2011) 69-74

19. S. Brimaud, Z. Jusys, and R.J. Behm, *Shape-selected nanocrystals for in situ spectro-electrochemistry studies on structurally well defined surfaces under controlled electrolyte transport: A combined in situ ATR-FTIR/online DEMS investigation of CO electrooxidation on Pt* Beilstein J. Nanotechnol. 5 (2014) 735-746

20. G.-Q. Lu, S.-G. Sun, S.-P. Chen, and L.-R. Cai, *Novel properties of dispersed Pt and Pd thin layers supported on GC for CO adsorption studied using in situ MS-FTIR reflection spectroscopy* J. Electroanal. Chem. 421 (1997) 19-23

21. S.-G. Sun and Y.-Y. Yang, *Studies of kinetics of HCOOH oxidation on Pt(100), Pt(110), Pt(111), Pt(510) and Pt(911) single crystal electrodes* J. Electroanal. Chem. 467 (1999) 121-131

22. A.E. Bjerke, P.R. Griffiths, and W. Theiss, *Surface-enhanced infrared absorption of CO on platinized platinum* Anal. Chem. 71 (1999) 1967-1974

23. S. Park, Y. Tong, A. Wieckowski, and M.J. Weaver, *Infrared reflection-absorption properties of platinum nanoparticle films on metal electrode substrates: control of anomalous optical effects* Electrochem. Commun. 3 (2001) 509-513

24. O. Wolter and J. Heitbaum, *Differential electrochemical mass spectroscopy (DEMS) - a new method for the study of electrode processes* Ber. Bunsenges. Phys. Chem. 88 (1984) 2-6

25. R.A. Martinez-Rodriguez, F.J. Vidal-Iglesias, J. Solla-Gullón, C.R. Cabrera, and J.M. Feliu, *Synthesis of Pt nanoparticles in water-in-oil microemulsion: effect of HCl on their surface structure* J. Am. Chem. Soc. 136 (2014) 1280-1283

26. J. Solla-Gullón, P. Rodríguez, E. Herrero, A. Aldaz, and J.M. Feliu, *Surface characterization of platinum electrodes* Phys. Chem. Chem. Phys. 9 (2007) 1359-1373

27. J. Solla-Gullón, E. Herrero, F.J. Vidal-Iglesias, J. Feliu, and A. Aldaz, *CO monolayer oxidation on semi-spherical and preferentially oriented (100) and (111) platinum nanoparticles* Electrochem. Commun. 8 (2006) 189-194

28. J. Solla-Gullón, F.J. Vidal-Iglesias, and J.M. Feliu, *Shape dependent electrocatalysis* Annu. Rep. Prog. Chem. , Sect. C: Phys. Chem. 107 (2011) 263-297

29. A. Vaskevich, M. Rosenblum, and E. Gileadi, *Underpotential-overpotential transition of silver overlayer on platinum Part 1. Formation of a Pt+Ag surface alloy* J. Electroanal. Chem. 383 (1995) 167-174

30. P. Carro, H. Creus, P. Schilardi, S. González, R.C. Salvarezza, and A.J. Arvia, *Topographic changes of polycrystalline Ag and Cu electrodes in acid aqueous solutions resulting from a prolonged application of the potential reversal technique* J. Electrochem. Soc. 143 (1996) 2294-2305

31. B.B. Blizanac, P.N. Ross, and N.M. Markovic, *Oxygen electroreduction on Ag (111): the pH effect* Electrochim. Acta 52 (2007) 2264-2271

32. M. Schweizer and D.M. Kolb, *Electrochemical and structure studies of ethanethiol self-assembled monolayers on Ag single crystal electrodes* J. Electroanal. Chem. 564 (2004) 85-91

33. N. Takehiro, P. Liu, A. Bergbreiter, J.K. Nørskov, and R.J. Behm, *Hydrogen adsorption on bimetallic PdAu(111) surface alloys: Minimum adsorption ensemble, ligand and ensemble effects, and ensemble confinement* Phys. Chem. Chem. Phys. 16 (2014) 23930-23942

34. L. A. Mancera, A. Bensch, A. K. Engstfeld, R. J. Behm, and A. Groß, *Intermixing of Pt and Cu atoms in PtCu/Ru(0001) surface alloys* (2016).

35. S. Koh and P. Strasser, *Electrocatalysis on bimetallic surfaces: Modifying catalytic reactivity for oxygen reduction by voltammetric surface dealloying* J. Am. Chem. Soc. 129 (2007) 12624-12625

36. P. Strasser, S. Koh, and J. Greeley, *Voltammetric surface dealloying of Pt bimetallic nanoparticles: an experimental and DFT computational analysis* Phys. Chem. Chem. Phys. 10 (2008) 3670-3683

37. P. Strasser and S. Kühl, *Dealloyed Pt-based core-shell oxygen reduction electro-catalysts* Nano Energy (2016) online available, DOI: 10.1016/j.nanoen.2016.04.04

38. C.R. Henry, *Surface studies of supported model catalysts* Surf. Sci. Rep. 31 (1998) 231-325

39. K. Kinoshita, in *Modern Aspects of Electrochemistry*, J. O. Bockris, B. Conway, and R. E. White, Eds. (Plenum Press, New York, 1982), Vol. 14.

40. Z. Peng, H. You, and H. Yang, *An electrochemical approach to PtAg alloy nanostructures rich in Pt at the surface* Adv. Funct. Mater. 20 (2010) 3734-3741

41. V.V. Pryadchenko, V.V. Srabionyan, E.B. Mikheykina, L.A. Avakyan, V.Y. Murzin, Y.V. Zubavichus, I. Zizak, V.E. Guterman, and L.A. Bugaev, *Atomic structure of bimetallic nanoparticles in PtAg/C catalysts: Determination of components distribution in the range from disordered alloys to "core-shell" structures* J. Phys. Chem. C 119 (2015) 3217-3227

42. H. Röder, R. Schuster, H. Brune, and K. Kern, *Monolayer-confined mixing at the Ag-Pt(111) interface* Phys. Rev. Lett. 71 (1993) 2086-2089

43. S. Brimaud and R.J. Behm, *Electro-deposition of a Pt monolayer film - Using kinetic limitations for atomic layer epitaxy* J. Am. Chem. Soc. 135 (2013) 11716-11719

44. G. Orozco, M.C. Pérez, A. Rincón, and C. Gutiérrez, *Adsorption and electrooxidation of carbon monoxide on silver* Langmuir 14 (1998) 6297-6306

45. M. Mavrikakis, B. Hammer, and J.K. Nørskov, *Effect of strain on the reactivity of metal surfaces* Phys. Rev. Lett. 81 (1998) 2819-2822

46. S. Brimaud, S. Pronier, C. Coutanceau, and J.M. Leger, *New findings on CO electrooxidation at platinum nanoparticle surfaces* Electrochem. Commun. 10 (2008) 1703-1707

47. T. Biegler, D.A.J. Rand, and R. Woods, *Limiting oxygen coverage on platinized platinum; relevance to determination of real platinum area by hydrogen adsorption* J. Electroanal. Chem. 29 (1971) 269-277

48. D. van der Vliet, C. Wang, D. Li, A.P. Pailikas, J. Greeley, R.B. Rankin, D. Strmcnik, D. Tripkovic, N.M. Markovic, and V. Stamenkovic, *Unique electrochemical adsorption properties of Pt-skin surfaces* Angew. Chem. 124 (2012) 3193-3196

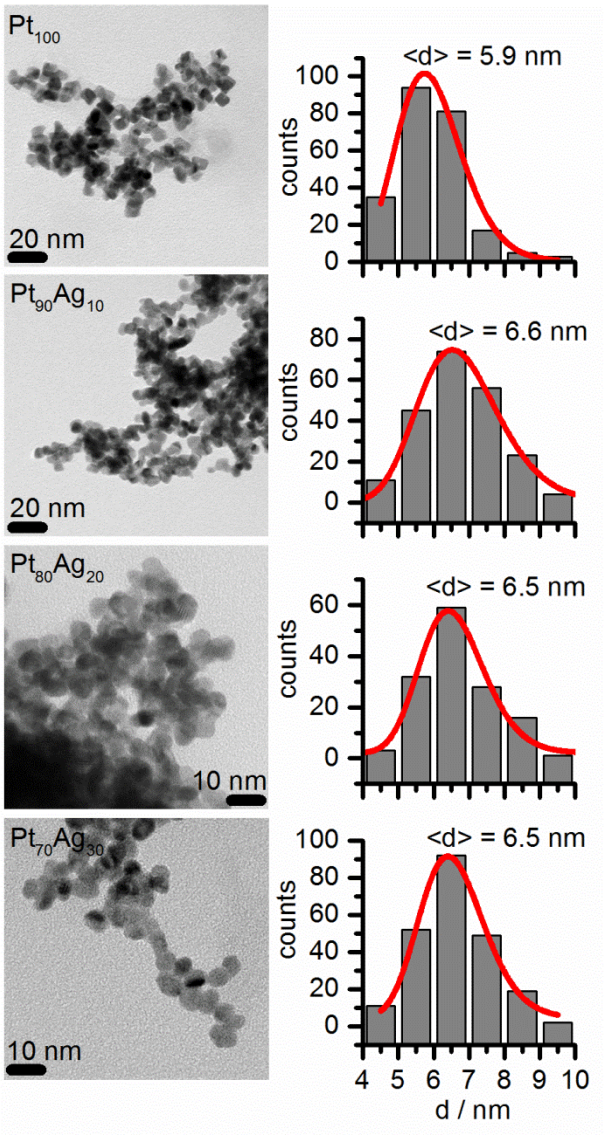

Figure 1 Representative BFTEM images (left column) and particle size distributions (right column) of Pt_{100}, $Pt_{90}Ag_{10}$, $Pt_{80}Ag_{20}$, and $Pt_{70}Ag_{30}$ nanoparticle samples (from top to bottom).

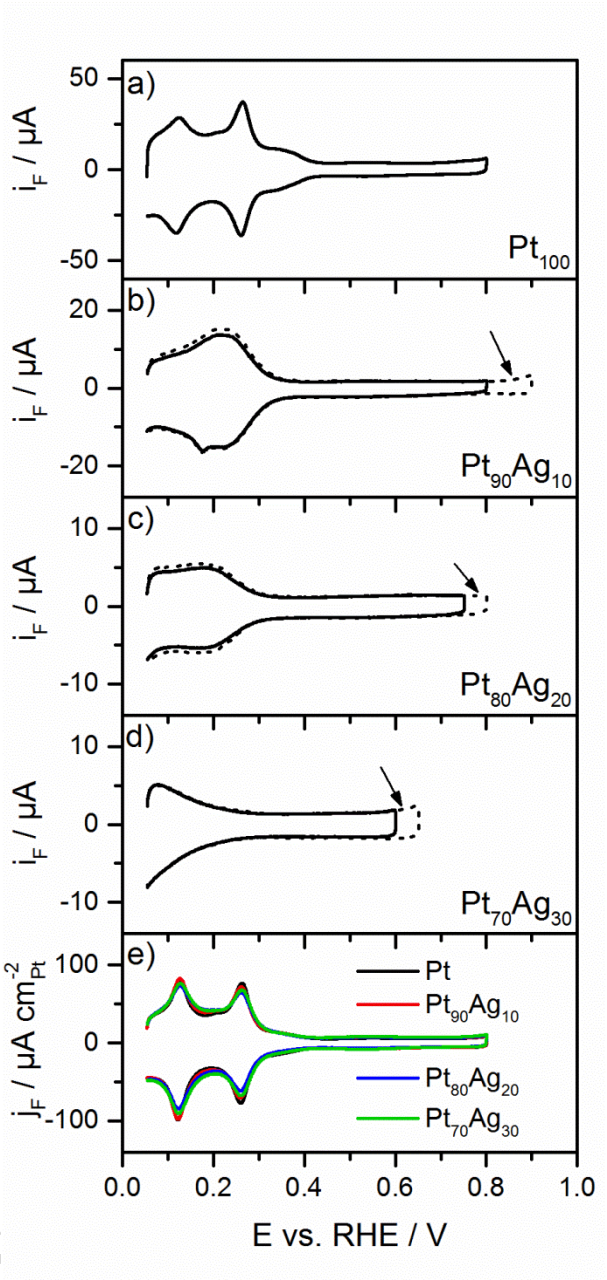

Figure 2 Cyclic voltammograms of a) Pt_{100}, b) $Pt_{90}Ag_{10}$, c) $Pt_{80}Ag_{20}$, and d) $Pt_{70}Ag_{30}$ nanoparticles with the upper potential limits just below (solid line) and just (dotted line) above the onset of potential-induced Ag dissolution . The arrows indicate the onset potential of Ag dissolution from the nanoparticle surface. e) cyclic voltammograms of the nanoparticle samples after electrochemical de-alloying (100 cycles between 0.05 and 1.45 V, scan rate 50 mV s^{-1}, in 0.5 M H_2SO_4).

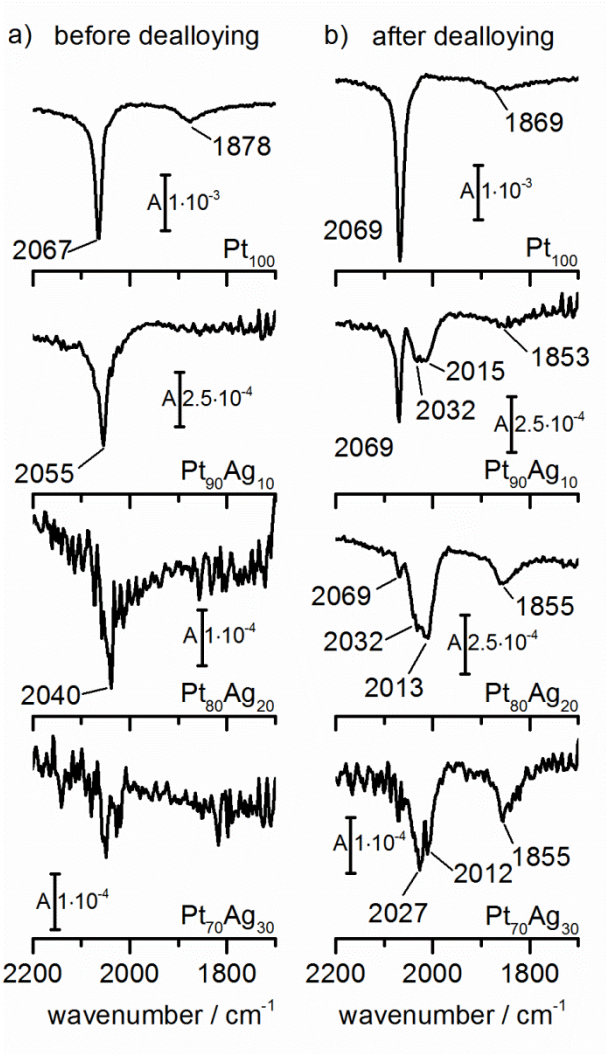

Figure 3 *In situ* IR vibrational spectra of a saturated CO adlayer after CO adsorption at E_{ads} = 0.10 V and removal of CO dissolved in the electrolyte (0.5 M H_2SO_4) on the Pt_xAg_{100-x} nanoparticle samples (see figure) before (left column) and after (right column) electrochemical de-alloying.

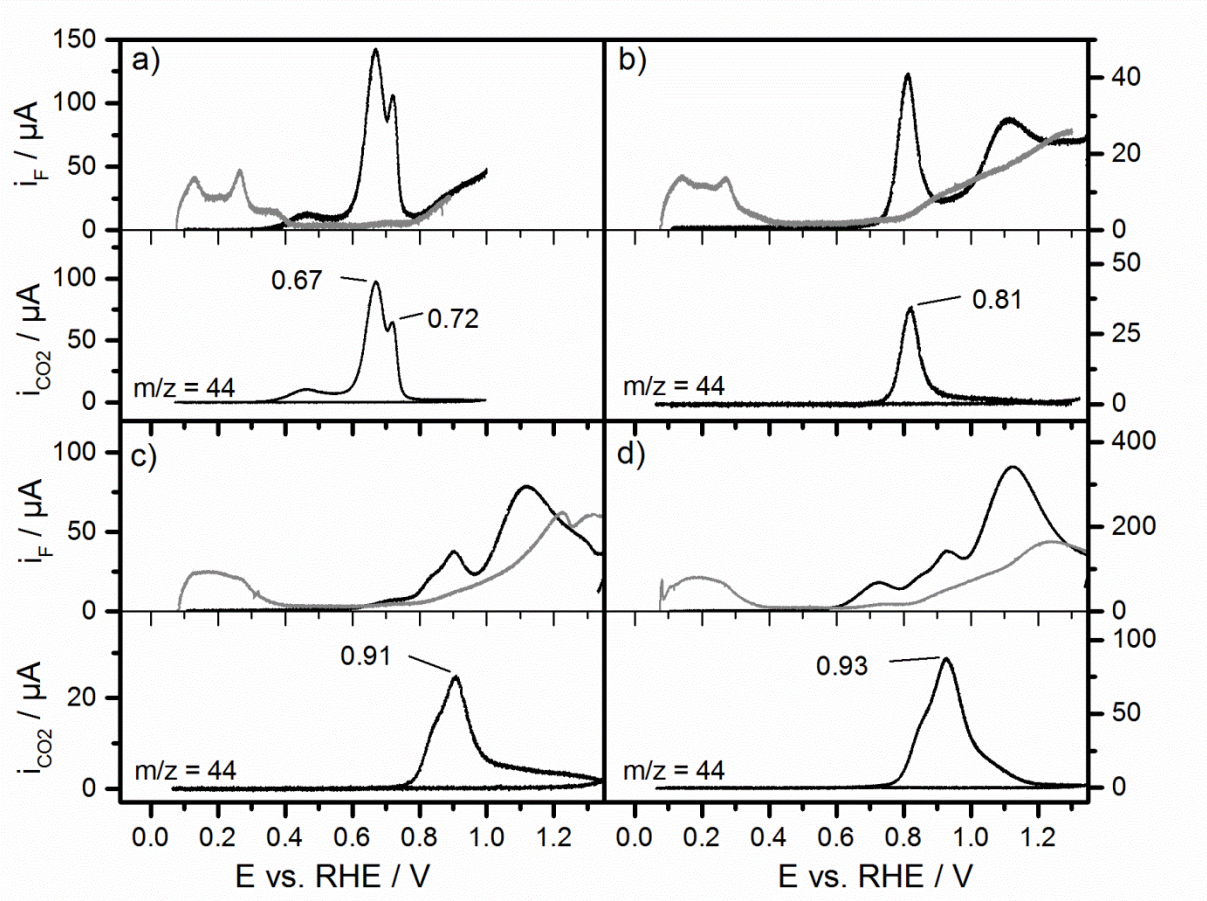

Figure 4 First (black lines) and second (grey lines) positive-going potential scans in CO_{ad} stripping voltammograms (top panels) and partial currents for CO_2 formation derived from the mass spectrometric CO_2 ion currents (m/z = 44) recorded simultaneously (bottom panels) of a saturated CO adlayer (E_{ads} = 0.10 V) on a) Pt_{100}, b) $Pt_{90}Ag_{10}$, c) $Pt_{80}Ag_{20}$, and d) $Pt_{70}Ag_{30}$ nanoparticle samples before electrochemical de-alloying (0.5 M H_2SO_4, 5 mV s^{-1}).

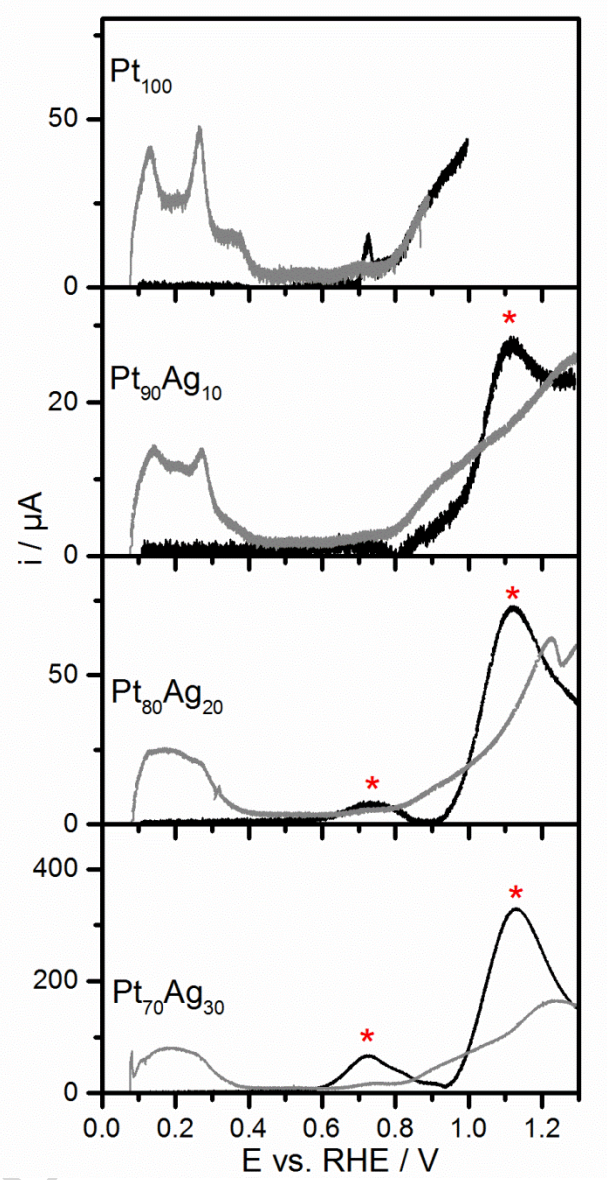

Figure 5 Partial Faradaic current for Ag dissolution during the first positive-going scan in the CO_{ad} stripping voltammograms on the as-prepared bimetallic Pt_xAg_{100-x} nanoparticles (see Fig. 4), including also the small contributions from double layer charging and Pt oxidation, which was calculated by subtracting the partial current for CO_2 formation from the total Faradaic current (black lines). Second positive-going potential scans in the CO_{ad} stripping voltammograms are indicated as grey lines (data from Fig. 4). Red stars indicate Ag dissolution peaks.

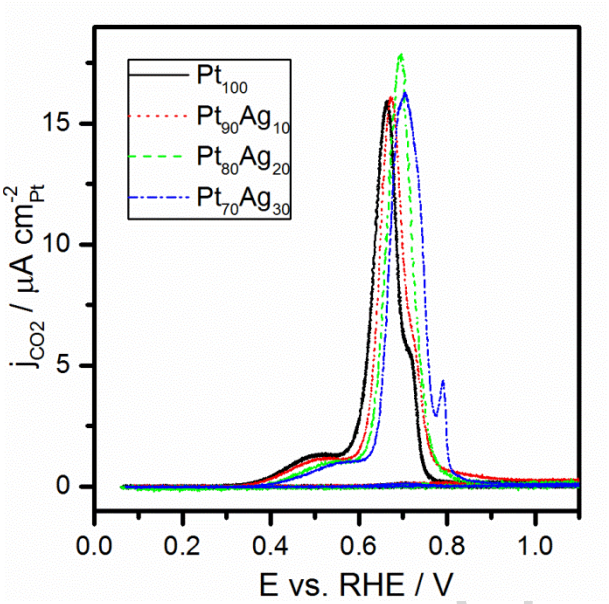

Figure 6 Current densities for CO_2 formation currents derived from the mass spectrometric currents (m/z = 44) during CO_{ad} stripping of a saturated CO adlayer (E_{ads} = 0.10 V, v = 5 mV s^{-1}) on the electrochemically de-alloyed bimetallic Pt_xAg_{100-x} nanoparticle samples.

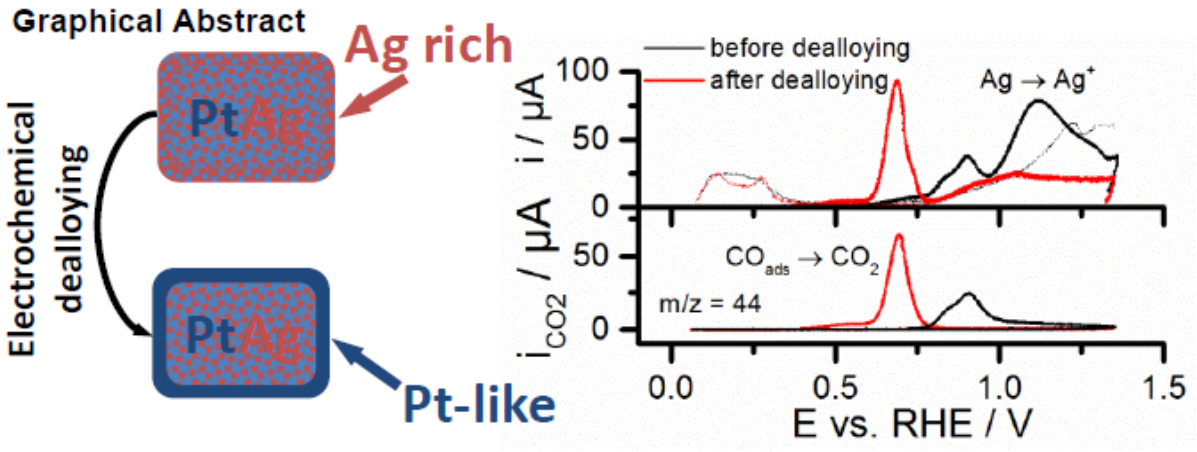

Highlights

- As-prepared PtAg nanoparticles are surface enriched in Ag which is highly dispersed
- Electrochemical de-alloying results in a Pt-like, but not Pt-identical surface
- H_{UPD} does not sense Pt_2Ag or $PtAg_2$ sites, not suitable for surface Pt determination
- CO adsorbs on all Pt ensembles , suitable for Pt surface determination
- Ag-induced modification of Pt properties are probed for CO adsorption and oxidation